JGP Journal of General Physiology

COMMUNICATION

Calcium has a direct effect on thick filament activation in porcine myocardium

Saffie Mohran[1,2,3], Timothy S. McMillen[2], Christian Mandrycky[1,2], An-Yue Tu[1,2,3], Kristina B. Kooiker[2,3,4,5], Wenjing Qian[6], Stephanie Neys[4], Brayan Osegueda[3], Farid Moussavi-Harami[2,3,4,5], Thomas C. Irving[7,8], Michael Regnier[1,2,3,5], and Weikang Ma[7,8]

Sarcomere activation in striated muscle requires both thin filament–based and thick filament–based activation mechanisms. Recent studies have shown that myosin heads on the thick filaments undergo OFF to ON structural transitions in response to calcium (Ca^{2+}) in permeabilized porcine myocardium in the presence of a small molecule inhibitor that eliminated active force. The changes in X-ray diffraction signatures of OFF to ON transitions were interpreted as Ca^{2+} acting to activate the thick filaments. Alternatively, Ca^{2+} binding to troponin could initiate a Ca^{2+}-dependent crosstalk from the thin filament to the thick filament via interfilament connections such as the myosin binding protein-C. Here, we exchanged native troponin in permeabilized porcine myocardium for troponin containing the cTnC D65A mutation, which disallows the activation of troponin through Ca^{2+} binding to determine if Ca^{2+}-dependent thick filament activation persists in the absence of thin filament activation. After the exchange protocol, over 95% of the Ca^{2+}-activated force was eliminated. Equatorial intensity ratio increased significantly in both WT and D65A exchanged myocardium with increasing Ca^{2+} concentration. The degree of helical ordering of the myosin heads decreased by the same amount in WT and D65A myocardium when Ca^{2+} concentration increased. These results are consistent with a direct effect of Ca^{2+} in activating the thick filament rather than an indirect effect due to Ca^{2+}-mediated crosstalk between the thick and thin filaments.

Introduction

Cardiac muscle contraction is highly regulated to fulfill a wide variety of the body's specific circulatory needs. Contractile activation had long been regarded as a calcium (Ca^{2+})-dependent, thin filament-based mechanism, where Ca^{2+} binding to the troponin complex allows mobilization of tropomyosin. This structural displacement of tropomyosin exposes myosin binding sites on F-actin to facilitate actomyosin binding (Tobacman, 1996; Gordon et al., 2000). It is now realized, however, that thick filament-based activation is also required during muscle contraction (Irving, 2017), but the mechanisms of this activation are not well understood.

There is strong evidence that in relaxed muscle, a large portion of the myosin heads reside in a quasi-helically ordered state close to the thick filament backbone while the myosin heads during contraction are more associated with actin (Huxley and Brown, 1967). One mechanism of activating resting myosin heads in the thick filament to permit contraction was introduced by Linari et al. (2015), who proposed a strain-dependent thick filament activation model ("mechano-sensing") derived from experiments on frog skeletal muscle (Linari et al., 2015) and later expanded to rodent myocardium (Reconditi et al., 2017; Brunello et al., 2020). In this model, thin filaments are activated by Ca^{2+} influx, and a small number of "constitutively ON" myosin heads can form crossbridges and generate a small amount of force. In this way, the thick filament acts as a mechanical sensor where the strain generated in the thick filament backbone by this amount of force can release myosin heads from an inactive quasi-helically ordered OFF state to an active disordered ON state thereby regulating the number of myosin heads competent to bind actin and generate force (Linari et al., 2015; Caremani et al., 2019b). In addition to the mechanosensing mechanism, multiple studies point to a titin-based thick filament strain mechanism in myofilament length-dependent activation (Irving et al., 2011; Ait-Mou et al., 2016; Ma et al., 2021; Hessel et al.,

[1]Department of Bioengineering, University of Washington, Seattle, WA, USA; [2]Center of Translational Muscle Research, University of Washington, Seattle, WA, USA; [3]Institute for Stem Cell and Regenerative Medicine, University of Washington, Seattle, WA, USA; [4]Division of Cardiology, Department of Medicine, University of Washington, Seattle, WA, USA; [5]Center for Cardiovascular Biology, University of Washington, Seattle, WA, USA; [6]College of Basic Medical Sciences, Dalian Medical University, Dalian, China; [7]BioCAT, Department of Biology, Illinois Institute of Technology, Chicago, IL, USA; [8]Center for Synchrotron Radiation Research and Instrumentation, Illinois Institute of Technology, Chicago, IL, USA.

Correspondence to Weikang Ma: wma6@iit.edu

This work is part of a special issue on Myofilament Structure and Function.

2022). It has been shown, however, that thick filament strain cannot be the only trigger for OFF to ON structural transitions that result in the release of myosin heads from the thick filament backbone (Ma et al., 2018b, 2023b; Park-Holohan et al., 2021; Brunello and Fusi, 2023).

We previously showed that myosin heads on the thick filaments undergo OFF to ON, order to disorder, and structural transitions in the thick filaments of permeabilized porcine myocardium in response to Ca^{2+} and in the absence of active force (Ma et al., 2022b). Ca^{2+}–mediated active contraction was abolished by incubating the myocardium with a small molecule thin filament inhibitor (MYK7660) that allowed Ca^{2+} binding to troponin C but inhibited force by increasing the release rate of Ca^{2+} to prevent downstream movement of tropomyosin (Ma et al., 2022b). The results were interpreted as direct Ca^{2+} activation of the thick filament. An alternative mechanism has subsequently been proposed where binding of Ca^{2+} to troponin initiates a Ca^{2+}-dependent "crosstalk" between thin and thick filaments via interfilament connections (Brunello and Fusi, 2023; Caremani et al., 2023; Short, 2023). For example, cardiac myosin binding protein-C (cMyBP-C), whose N terminus can bind to the thin filaments, could act as a conduit for any Ca^{2+}-mediated signals to the thick filament. Given that MYK7660 allows the binding of Ca^{2+} to troponin, such mechanisms cannot be excluded from the previous studies. To critically test the "crosstalk" hypothesis, we exchanged native troponin in permeabilized porcine myocardium for troponin containing the cTnC D65A mutation. This mutation inhibits troponin activation caused by Ca^{2+} binding at the N-terminal "trigger" site of cTnC (Gillis et al., 2007; Little et al., 2012). We observed that the changes in X-ray diffraction signatures indicative of OFF to ON transitions in response to increased Ca^{2+} concentration are still present in porcine myocardium with the D65A cTnC. These results are consistent with a direct effect of Ca^{2+} in activating the thick filament rather than an indirect effect due to Ca^{2+}-mediated crosstalk between the thick and thin filaments.

Materials and methods

Recombinant protein mutagenesis and purification

Methods for construction and expression of wild type (WT) rat cTnC, cTnI, and cTnT in pET24a vectors were developed previously in our laboratory (Potter, 1982; Köhler et al., 2003). The cTnC (D65A) mutant was constructed from the rat WT cTnC plasmid using a Quikchange site-directed mutagenesis kit from Stratagene and confirmed by DNA sequence analysis. The plasmids for cTnC variants were then transformed into *Escherichia coli* BL21 cells. Proteins were expressed and purified following the protocols developed as described previously (Dong et al., 1996).

Recombinant cTnC labeling and steady-state fluorescence measurements

Methods for cTnC labeling and fluorescence measurements were previously described (Wang et al., 2012, 2013). Briefly, purified WT and D65A cTnC were labelled with a fluorescent probe {*N*-[2-(iodoacetoxy)ethyl]-*N*-methylamino-7-nitrobenz-2-oxa-1,3-diazole (IANBD, M_w = 406.14, Cat No: I-9; Life technologies)}. at position C84 in the dark overnight at 4°C. IANBD enables the quantification of Ca^{2+}–cTnC (K_{Ca}) binding affinities. The labeling efficiency was obtained by comparing the IANBD fluorophore versus protein concentration ratio. The IANBD fluorophore concentration was computed using the maximal absorbance of labeled protein at a wavelength of 481 nm and dividing by IANBD's extinction coefficient (21,000 M^{-1} cm^{-1}). The steady-state fluorescence measurements were recorded by a luminescence spectrometer at 530 nm (LS50B; PerkinElmer) at room temperature with 150 mM KCl, 20 mM MOPS, 3 mM $MgCl_2$, 2 mM EGTA, and 1 mM DTT (pH 7.0). The emission signal was then recorded during the titration of microliter amounts of Ca^{2+} into 2 ml of WT or D65a cTC (0.3 µM). The concentration of free Ca^{2+} was computed using Maxchelator (Bers et al., 2010). Titration curve data were fitted with the Hill equation.

Reconstitution of troponin complexes

Reconstitution of the cardiac troponin complex was performed as described previously (Potter, 1982; Korte et al., 2012). Briefly, the cTn subunits cTnI and cTnT were first dialyzed independently against 6.0 M urea, 25 mM TRIS, and 1.0 mM EDTA at pH 8.0. After dialysis, cTnC (WT or D65A mutant) was mixed with both the cTnI and cTnT proteins at a molar ratio of 1:1:1 in the presence of 1.5 mM $CaCl_2$. The protein solutions were then incubated at room temperature for 30 min. After incubation, solutions were dialyzed through a series of five steps to lower the ionic strength. All solutions contained 20 mM MOPS, 3.0 mM $MgCl_2$, and 2.0 mM EGTA at pH 7.0. The progress was from 2.0 M urea, 0.75 M KCl to 0 and 0.15 M, respectively, with an additional 1.0 mM DTT in the final solution. All dialyses were done at 4°C in the dark without stirring. Proteins that precipitated during the dialysis with decreasing KCl concentration were removed by centrifugation. The final troponin complex concentration (mg/ml) was determined using a spectrofluorometer (Beckman) by dividing the observed OD value collected at 280 nm by the extinction coefficient (0.45).

Porcine myocardium preparations

Porcine myocardium from three hearts for the X-ray diffraction experiments was permeabilized as described previously (Ma et al., 2022a, 2023a). Briefly, previously frozen muscles were permeabilized in a skinning solution (pCa 8.0 solution [91 mM K^+-propionate, 3.5 mM $MgCl_2$, 0.16 mM $CaCl_2$, 7 mM EGTA, 2.5 mM Na_2ATP, 15 mM creatine phosphate, 20 mM imidazole, and 1% protease inhibitor cocktail at pH 7.0] plus 15 mM 2,3-butanedione monoxime, 1% Triton-X100) overnight at 4°C. The fiber bundles were further dissected into preparations with a length of 5 mm with a diameter of ~200 µm prior to the attachment of aluminum T-clips to both ends in pCa 8 solution. The preparations were randomly separated into the WT and D65A groups. The number of technical replicates was 20 for WT and 40 for the D65A exchanged myocardium. Preparations were then washed three times in pCa 8.0 solutions containing 1 mg/ml BSA. After washing, preparations were placed in pCa 8.0 solution with 3% dextran on ice.

Troponin complex exchange

Passive exchanges of whole WT or D65A cTn complex into dissected porcine strips were done as described previously (Korte et al., 2012). Briefly, t-clipped porcine strips were incubated for 16 h in a 4°C fridge on a mechanical rocker (Beckman) with troponin exchange solution (~1 mg/ml recombinant WT or D65A cTn, 4 mM ATP, 1 mg/ml DTT, and 1% protease inhibitor cocktail). Exchange solutions were refreshed at 8 h to increase exchange efficiency. Preparations were then washed three times in pCa 8.0 solutions containing 1 mg/ml BSA. After washing, preparations were placed in pCa 8.0 solution with 3% dextran on ice. Samples were used within 12 h after washing. Note that the exchanges of WT and D65A cTn complexes were done under identical conditions so that the results can be compared.

X-ray diffraction measurements

X-ray diffraction experiments were performed at the BioCAT beamline 18ID at the Advanced Photon Source, Argonne National Laboratory (Fischetti et al., 2004). The X-ray beam energy was set to 12 keV (0.1033 nm wavelength) at an incident flux of ~5×10^{12} photons per second. The specimen-to-detector distance was ~3 m. The muscles, bound on each end by aluminum foil T-clips, were attached to a hook on a force transducer (Model 402B; Aurora Scientific Inc.) and a static hook inside a customized chamber. The solution was maintained between 28°C and 30°C with a heat exchanger attached to the bottom of the chamber. The muscles were stretched to a sarcomere length of 2.3 µm as measured by light diffraction with a helium-neon laser (633 nm). X-ray patterns were collected at pCa 8.0, pCa 5.8, and pCa 4.5 in the presence of 3% dextran using a MarCCD 165 detector (Rayonix Inc.) with a 1-s exposure time. The muscle samples were oscillated along their horizontal axes at a velocity of 1–2 mm/s to minimize radiation damage. The irradiated areas are moved vertically after each exposure to avoid overlapping X-ray exposures. The force-pCa data were monitored using a Dynamic Muscle Control system (v5.5) from Aurora Scientific Inc., and absolute forces (mN) without correcting for the cross-sectional area are reported in this manuscript.

X-ray data analysis

The data were analyzed using the MuscleX software package developed at BioCAT (Jiratrakanvong et al., 2024). Three to four patterns were collected under each condition, and spacings and intensities of X-ray reflections extracted from these patterns were averaged. The equatorial reflections were measured by the "Equator" routine in MuscleX to calculate the equatorial intensity ratio, $I_{1,1}/I_{1,0}$, and interfilament lattice spacing, $d_{1,0}$, as described previously (Ma et al., 2018a). The intensities and spacings of meridional and layer line reflections were measured using the "Projection Traces" routine in MuscleX after the patterns were quadrant-folded and the diffuse scattering subtracted to improve the signal-to-noise ratio as described previously (Ma et al., 2018a, 2020). There were no significant changes in the radial width of the M3 reflection during activation, thus no correction for width was applied to the measured intensities. To compare the intensities under different conditions, the measured intensities of X-ray reflections were normalized to the sixth-order actin-based layer line intensities as described previously (Ma et al., 2022b). Statistical analyses were performed using GraphPad Prism 10 (GraphPad Software). The results were given as mean ± SEM. Statistical comparisons under each condition were done using nested *t* tests. Symbols on figures represent: *: P < 0.05, **: P < 0.01, ***: P < 0.001, ****: P < 0.0001.

Results

The steady-state fluorescence measurements performed on purified and IANBD-labeled cTnC proteins provide significant insights into the structural change that occurs to cTnC during Ca^{2+} binding. In Ca^{2+}-free environments, the IANBD probe, located at site C84, is buried within the protein structure. Upon the binding of Ca^{2+}, activation of cTnC exposes the IANBD probe, thus increasing the fluorescent readout captured by the spectrofluorometer. These results are observed in the WT cTnC experiments, as the fluorescent change increased by ~65% from baseline (no Ca^{2+}) measurements. Interestingly, measurements performed with purified D65A cTnC showed a fluorescent decrease of ~20% (Fig. 1 A). These measurements would suggest Ca^{2+} may interact in some way with cTnC but not in a manner that promotes the conformational change seen when Ca^{2+} binds in site II and results in exposure of the hydrophobic patch, essential for thin filament activation. These experiments establish that D65A cTnC is not competent to activate the thin filaments in the presence of Ca^{2+}.

Inhibition of thin filament activation by D65A cTnC was observed when we exchanged native porcine cTn complex with recombinant rat cTn containing the WT or D65A cTnC mutation. Exchanged tissues eliminated >95% of the active force with D65A cTnC exchange compared to preparations with WT cTnC at both pCa 5.8 (95.6%, 0.316 ± 0.02 mN in WT group versus 0.014 ± 0.01 mN in D65A group, P = 0.02) and pCa 4.5 (96.3%, 1.20 ± 0.13 mN in WT group versus 0.041 ± 0.02 mN in D65A group, P < 0.0001) (Fig. 1 B).

We then examined the structural transitions of the WT or D65A exchanged permeabilized porcine cardiac myocardium tissues in response to different Ca^{2+} concentrations using small-angle X-ray diffraction (Fig. 2 A). At high Ca^{2+} concentration (pCa 4.5), the intensities of all the myosin-based reflections (M3, M6, MLLs in Fig. 2 A) become weaker compared with low Ca^{2+} concentration (pCa 8.0) in tissues exchanged with either WT or D65A cTn. The interfilament lattice spacing, $d_{1,0}$, decreased as the Ca^{2+} concentration increased in both WT and D65A groups with no significant difference between the two groups at each Ca^{2+} concentration (Fig. 2 B). The equatorial intensity ratio, $I_{1,1}/I_{1,0}$, is an indicator of the proximity of myosin heads to actin in relaxed muscle and is closely correlated to the number of force-producing crossbridges in activated muscle (Haselgrove and Huxley, 1973; Matsubara, 1980; Ma et al., 2018a, 2020). In the low Ca^{2+} resting state (pCa 8.0), $I_{1,1}/I_{1,0}$ was slightly but significantly lower in D65A group (0.32 ± 0.008) compared with WT group (0.37 ± 0.01, P = 0.04). $I_{1,1}/I_{1,0}$ increased to (0.51 ± 0.02) and (0.64 ± 0.03) pCa 5.8 and pCa 4.5, respectively, from the WT group. In the D65A group, where Ca^{2+} mediated troponin activation is mostly abolished, $I_{1,1}/I_{1,0}$ increased to (0.40 ± 0.012) and

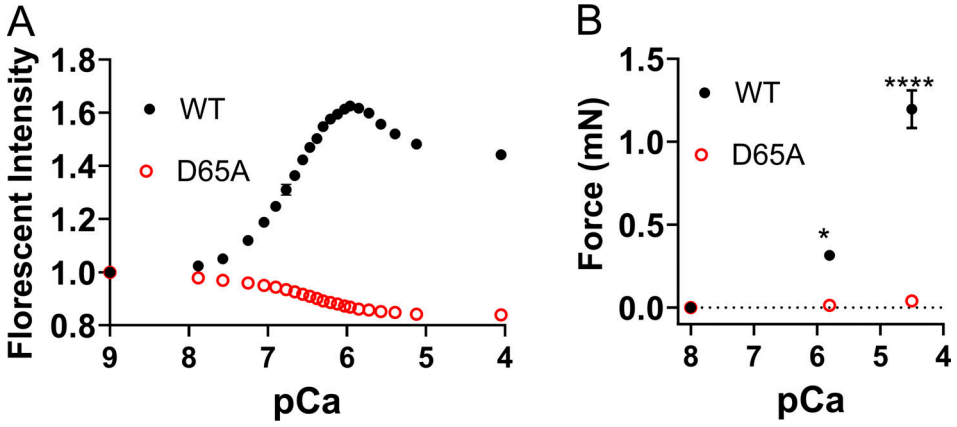

Figure 1. **The D65A mutation in cTnC inhibits activation of troponin in the presence of calcium. (A)** Normalized steady-state fluorescent emission change of purified and IANBD-labeled WT (black) and D65A (red) cTnC at increasing concentrations of calcium. **(B)** Force generation of permeabilized porcine myocardium strips with exchanged rat WT or D65A full troponin complex at submaximal (pCa 5.8) and maximal (pCa 4.5) calcium.

(0.45 ± 0.014) pCa 5.8 and pCa 4.5, respectively. The radius of the center of mass of the cross-bridges (R_m), which directly measures the proximity of the helically ordered myosin heads on the surface of the thick filament backbone (Ait-Mou et al., 2016; Ma et al., 2018a), was significantly larger in WT (16.06 ± 0.22) group than D65A group (15.30 ± 0.14, P = 0.0039) at pCa8.

Under resting conditions (pCa 8.0), most of the myosin heads are quasi-helically ordered on the surface of the thick filament, producing the myosin-based layer lines (MLLs). Myosin in resting muscle also has a ~14.3 nm axial periodicity along the thick filament, which gives rise to the third-order myosin-based meridional reflection (M3). The intensity of the first-order myosin-based layer line (I_{MLL1}) and the M3 reflection (I_{M3}) progressively decreased when Ca^{2+} concentrations increased, and there were no significant differences in I_{M3} and I_{MLL1} between the WT group where active actin-binding crossbridges were present and the D65A group where active contraction was mostly abolished (Fig. 3, A and B). The spacing of the M3 reflection (S_{M3}) and M6 reflection (S_{M6}) reports the axial periodicity of quasi-helically arranged myosin heads and structures

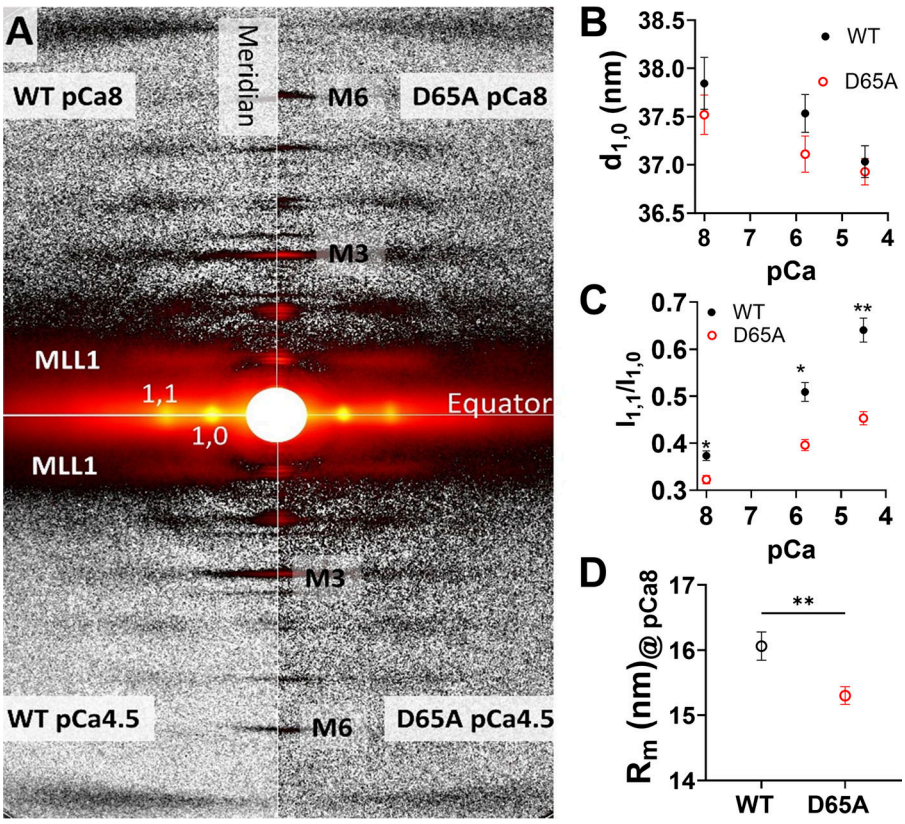

Figure 2. **Myosin heads are more closely associated with actin in the presence of calcium. (A–C)** Representative X-ray diffraction patterns from permeabilized porcine myocardium under resting (pCa 8.0) and activated (pCa 4.5) state from WT and D65A. **(B and C)** Lattice spacing ($d_{1,0}$) (B) and equatorial intensity ratio ($I_{1,1}/I_{1,0}$) (C) change at different Ca^{2+} concentrations from WT (black) and D65A (red). **(D)** The radius of the center of mass of the crossbridges, R_m, at pCa 8.

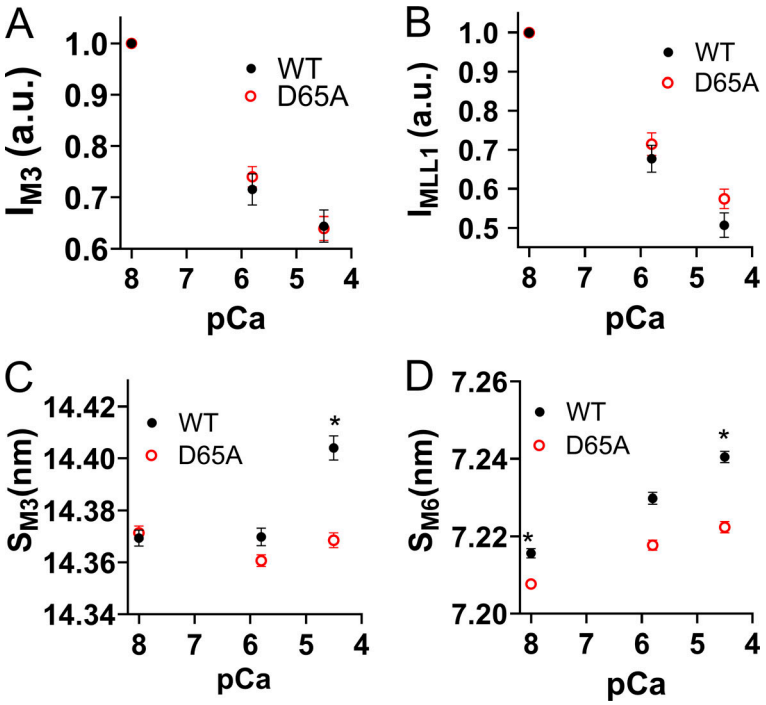

Figure 3. **Thick filament structural changes in the presence of calcium. (A)** The intensity of the third-order of myosin-based meridional reflection (I_{M3}) from permeabilized porcine myocardium under resting (pCa 8.0) and activated (pCa 4.5) state from WT and D65A. **(B)** The first-order myosin-based layer line (I_{MLL1}) from permeabilized porcine myocardium under resting (pCa 8.0) and activated (pCa 4.5) state from WT and D65A. **(C and D)** The spacing of the third (C) and sixth-order (D) myosin-based meridional reflections (S_{M3} and S_{M6}, respectively) from permeabilized porcine myocardium under resting (pCa 8.0) and activated (pCa 4.5) state from WT and D65A.

within the thick filament backbone, respectively (Reconditi, 2006). In the WT group, S_{M3} was 14.369 ± 0.003 nm and 14.370 ± 0.003 nm at pCa 8.0 and pCa 5.8, respectively, and it increased to 14.404 ± 0.005 nm at pCa 4.5. In the D65A group, S_{M3} decreased from 14.371 ± 0.003 nm at pCa 8.0–14.361 ± 0.003 nm at pCa 5.8 and increased to 14.369 ± 0.003 nm at pCa 4.5 (Fig. 3 C). Increased S_{M6} is associated with fewer myosin heads in the quasi-helically ordered state (Ma et al., 2023b) and vice versa (Ma et al., 2021), so changes in S_{M6} have been proposed as another indicator of OFF to ON transitions (Linari et al., 2015). S_{M6} was significantly larger in WT (7.215 ± 0.001 nm) than in D65A (7.208 ± 0.001, P = 0.02) at pCa 8.0. This difference persists as Ca^{2+} concentration increases (Fig. 3 D). S_{M6} increased to 7.230 ± 0.002 nm in WT and 7.218 ± 0.001 in D65A (P = 0.09) at pCa 5.8 and future increased to 7.240 ± 0.001 nm in WT and 7.222 ± 0.001 in D65A (P = 0.09) at pCa 4.5. The larger S_{M6} changes in the WT group (0.2% and 0.36% at pCa 5.8 and pCa 4.5, respectively) are expected because it involves both the release of the myosin heads from the OFF state and the increase in strain on the thick filament by active contraction (Reconditi et al., 2019). The increase in S_{M6} for the D65A (0.14% and 0.20% at pCa 5.8 and pCa 4.5, respectively), however, is solely from the OFF to ON transition of the thick filament in response to increasing Ca^{2+} (Fig. 3 D).

Discussion

There is a growing appreciation that Ca^{2+}, in addition to regulating the thin filaments through the troponin–tropomyosin system, may also regulate the movement of myosin heads relative to the thick filaments. However, many details regarding the mechanisms involved in thick filament activation are not known. A recent study decoupled the Ca^{2+}-mediated force production from Ca^{2+}-mediated regulation of the thick filaments by eliminating Ca^{2+}-mediated tropomyosin movement via a small-molecule thin filament inhibitor (MYK 7660; Bristol Meyers Squibb). Structural changes in thick filaments in response to Ca^{2+} in the presence of the inhibitor were interpreted as an indication that the thick filaments in porcine myocardium could sense and respond directly to Ca^{2+} through a mechanism that is not yet clear (Ma et al., 2022b). Additionally, Caremani et al. (2023) showed that increasing Ca^{2+} can lead to a loss of ordering of myosin heads, and this loss of ordering is more sensitive to Ca^{2+} than to force in rabbit skeletal muscle. In contrast, our previous studies of porcine cardiac muscle showed that the pCa_{50} for the loss of ordering, as indicated by loss of layer line intensity, was very similar to that for force development. It has been proposed that the OFF to ON transitions observed in the previous studies (Ma et al., 2022b; Caremani et al., 2023) could be explained by an alternative mechanism where binding of Ca^{2+} to troponin initiates a Ca^{2+} dependent "crosstalk" between the thin filaments and the thick filaments via interfilament connections (Brunello and Fusi, 2023; Caremani et al., 2023; Short, 2023). The aim of this current study was to investigate whether Ca^{2+}-mediated thick filament activation is a direct effect of Ca^{2+} on thick filaments or an indirect effect due to Ca^{2+}-mediated crosstalk via connecting structures between the thick and thin filaments.

In the D65A cTn group, small amounts of active force (<5% of WT) were detected at both submaximal and maximal Ca^{2+} (pCa 5.8 and pCa 4.5, respectively). This is most likely due to incomplete troponin exchange. We have established in the previous study, where active force was totally abolished, that the Ca^{2+}-dependent OFF to ON transition in porcine myocardium is independent of force (Ma et al., 2022b). The OFF to ON structural transitions in porcine myocardium, in the absence of active

force, show the exact same response to Ca^{2+} as for active force indicating that the structural transitions can be precisely modulated in a graded manner by Ca^{2+} concentration while the OFF to ON structural transitions in fast skeletal muscle is a quasi-stepwise process (Gong et al., 2022; Zhao et al., 2024). If these graded OFF to ON transitions in porcine myocardium are due to a putative Ca^{2+}-troponin initiated crosstalk pathway, the degree of myosin head activation would need to be correlated with the number of troponins with bound Ca^{2+} to result in the graded response we observed in porcine cardiac muscle here. In the current study, the <5% residual force roughly indicates that <5% of native troponins are unexchanged and it seems highly unlikely that a communication pathway involving only <5% of troponins with bound Ca^{2+} could result in 100% of the heads undergoing OFF to ON transitions as observed at maximum Ca^{2+} concentration. We believe, therefore, that the residual (<5%) active force developed in the D65A group as compared with the WT group will not affect the main conclusions drawn in this study. At pCa 8.0, $I_{1,1}/I_{1,0}$, R_m, and S_{M6} were significantly lower in the D65A group indicating that myosin heads adopt more inactive OFF states and are more associated with the thick filament backbone in the D65A group. Although we cannot exclude the possibility that exchanging WT cTn and D65A cTn could cause myofilament structural changes that are independent of Ca^{2+}, these results could be explained if a small amount of Ca^{2+} binds to a few cTnC N-terminal binding sites at pCa 8.0 in the WT group. Although this should be insufficient to result in active force production, it could potentially be sufficient to maintain a small number of myosin heads in the ON state where they can interact with actin, perhaps aided through electrostatic forces (Ma et al., 2023b). In the D65A group, however, any residual actomyosin interactions should be eliminated as the number of open myosin binding sites on the thin filaments will be greatly reduced resulting in more myosin heads remaining in the OFF state. The increases of $I_{1,1}/I_{1,0}$ and $S_{M6,}$ as Ca^{2+} concentrations increased, were larger in the WT group than in the D65A group. The increases of $I_{1,1}/I_{1,0}$ seen in the WT group can be explained by both the release of OFF states myosin heads and the binding of myosin heads to actin. The larger S_{M6} changes in the control group can be attributed to both the release of OFF states myosin heads and the increase in strain on the thick filament by force-producing crossbridges (Reconditi et al., 2019; Ma et al., 2023b). Here, the majority of the troponin units along the thin filament are deactivated by D65A troponin exchange while the thick filament OFF/ON response was unaffected, as indicated by the indistinguishable decreases of I_{MLL1} and I_{M3} in both the WT and D65A groups, as Ca^{2+} concentration increases. These results indicate that a direct effect of Ca^{2+} on the myosin in the thick filaments, in the absence of significant numbers of strong force-bearing crossbridges, can account for the majority of the OFF-to-ON transitions of myosin heads consistent with the findings from the previous study (Ma et al., 2022b) and in contradiction to the crosstalk hypothesis. Additionally, the lattice spacing decreases by ~0.5 nm between pCa 8 and pCa in both WT and D65A exchanged myocardium. A decrease in spacing cannot be explained by a decrease in sarcomere length due to internal shortening. Lattice spacing in skinned muscle depends on a balance of several opposing forces (Millman, 1998) so it is very difficult to devise unique explanations for spacing changes in resting skinned muscle. Without detailed knowledge of how radial forces might change with length in resting muscle, it is premature to attempt to propose a detailed mechanism for these changes in lattice spacing.

It has shown that in skeletal muscle, S_{M3} increased >1% during maximum activation (Reconditi, 2006; Caremani et al., 2023), which has been widely interpreted as a structural indicator of myosin heads adopting an ON state (Irving, 2017). Here, we show that S_{M3} in porcine myocardium increases significantly (0.21%) at pCa 4.5 in the WT group while in the D65A group, S_{M3} shows a significant decrease at pCa 5.8 with no increase at pCa 4.5. These data suggest that S_{M3} in porcine myocardium does not increase when myosin heads transition from an OFF to ON state in the absence of significant active force. This implies that the increase in S_{M3} during contraction seen in other muscle types is not a reliable indicator of myosin transitioning to the ON state in porcine myocardium. We speculate that when an increase of S_{M3} is observed, at least in porcine cardiac muscle, it is the result of a significant fraction of the myosin heads adopting a longer periodicity upon binding to actin (Zhao et al., 2024). This hypothesis is supported by the increase of S_{M3} in porcine cardiac muscle only at pCa 4.5 in the WT group where a significant number of force-producing crossbridges will be bound to actin. Increases in the thick filament backbone spacing, $S_{M6,}$ have also been used as an indicator of structural OFF to ON transitions, but a more detailed interpretation has been difficult. While S_{M6} has been shown to be responsive to strain in the thick filaments, albeit in a complex and non-linear way (Ma et al., 2018b), we and other investigators, however, have seen multiple situations where S_{M6} spacing can change without necessarily changing the tension on the thick filament (Caremani et al., 2019a, 2023; Ma et al., 2022b, 2023b, 2024a; Jani et al., 2024), indicating that S_{M6} can also reflect strain independent structural changes. Without differentiating between these two mechanisms, however, an increase in M6 has consistently been associated with an OFF-to-ON transition in all studies to date and is consistent with the other data presented here.

One question raised from the current and previous study (Ma et al., 2022b) is whether this phenomenon observed under steady state is rapid enough to be meaningful during normal heartbeats in vivo. A preliminary study (Ma et al., 2024b) showed that myosin heads leave their OFF state when filament stress is eliminated by zero load shortening during a normal twitch in intact pig trabeculae. We show here that thick filaments are still sensitive to increasing Ca^{2+} after greatly reducing the numbers of troponin competent to bind Ca^{2+} and participate in any Ca^{2+}-dependent interfilament crosstalk pathways. Taken together, it seems that at least some direct Ca^{2+}-dependent thick filament activation operates on a beat-by-beat basis in the heart. Another question that needs to be resolved in the future is where are the Ca^{2+} binding or sensing sites? At this time, we cannot pinpoint the Ca^{2+} binding or sensing sites on the thick filament that are responsible for this Ca^{2+}-mediated thick filament activation pathway. Our previous study (Ma et al., 2022b) showed that Ca^{2+} can destabilize the SRX states of synthetic

myosin filament, indicating that this Ca^{2+}-dependent transition is an intrinsic property of the myosin filament. We suggested that the F-hand motif of RLC might be the Ca^{2+} binding or sensing site for this Ca^{2+}-mediated thick filament activation pathway. Other sarcomeric proteins such as myosin-binding protein C and titin are also known to bind to Ca^{2+} (Labeit et al., 2003). It is possible that binding of Ca^{2+} to either myosin-binding protein C or titin can disrupt their interactions with myosin as indicated by recent high-resolution cryo-EM C-zone thick filament structures in the presence of mavacamten (Dutta et al., 2023). These hypotheses need to be tested in future studies.

Thick filament dysregulation appears to be the basis of many cardiomyopathies (Spudich, 2019; Nag and Trivedi, 2021), so a better understanding of thick filament regulation mechanisms could help us identify therapeutics necessary to mitigate these diseases. In this study, we provide strong corroboration of our previous demonstrations that Ca^{2+} can directly activate the thick filament. In so doing, Ca^{2+} can coordinate the excitation and contraction of cardiomyocytes. Imbalances in Ca^{2+} homeostasis have been shown to lead to cardiac disorders (Luo and Anderson, 2013). For one example, hypertrophic cardiomyopathy (HCM) can be caused by having more myosin heads in the ON state under resting conditions (Anderson et al., 2018; Spudich, 2019; Nag and Trivedi, 2021), and it has also been shown that intracellular diastolic Ca^{2+} concentration may be higher in HCM cells (Coppini et al., 2018). With our new understanding that Ca^{2+} plays a role in thick filament activation, it is worth considering that elevated diastolic Ca^{2+} concentration may result in more myosin heads in the ON state, further exacerbating the thick filament dysregulation in HCM cells. Our findings suggest that the Ca^{2+}-mediated thick filament activation pathway should be considered when investigating the pathological bases of sarcomere-based diseases and developing future drug candidates to treat these diseases.

Data availability

The datasets generated or analyzed during this study are included in this article. The raw data are available from the corresponding author upon reasonable request.

Acknowledgments

Henk L. Granzier served as editor.

This project is supported by grants 1R01HL171657 (W. Ma) and 5R01HL157169 (F. Moussavi-Harami) from National Heart Lung and Blood Institute, P30 GM138395 from the National Institute of General Medical Sciences (T.C. Irving) and P30 AR074990 from the National Institute of Arthritis and Musculoskeletal and Skin Diseases (M. Regnier) of the National Institutes of Health (NIH). This research used resources from the Advanced Photon Source, a U.S. Department of Energy (DOE) Office of Science User Facility operated for the DOE Office of Science by Argonne National Laboratory under Contract No. DE-AC02-06CH11357. The content is solely the authors' responsibility and does not necessarily reflect the official views of the NIH.

Author contributions: S. Mohran: Conceptualization, Data curation, Formal analysis, Investigation, Writing—original draft, T.S. McMillen: Formal analysis, Investigation, C. Mandrycky: Data curation, Investigation, Writing—review & editing, A.-Y. Tu: Resources, K.B. Kooiker: Investigation, W. Qian: Formal analysis, S. Neys: Investigation, B. Osegueda: Investigation, Visualization, F. Moussavi-Harami: Conceptualization, Funding acquisition, Writing—review & editing, T.C. Irving: Funding acquisition, Project administration, Resources, Supervision, Writing—original draft, Writing—review & editing, M. Regnier: Conceptualization, Data curation, Funding acquisition, Methodology, Project administration, Resources, Supervision, Validation, Visualization, Writing—review & editing, W. Ma: Conceptualization, Data curation, Formal analysis, Funding acquisition, Investigation, Methodology, Project administration, Resources, Software, Supervision, Validation, Visualization, Writing—original draft, Writing—review & editing.

Disclosures: T.C. Irving reported personal fees from Edgewise Therapeutics and grants from Bristol Meyers Squibb outside the submitted work. W. Ma reported personal fees from Edgewise Therapeutics outside the submitted work. No other disclosures were reported.

Submitted: 18 January 2024
Revised: 3 August 2024
Accepted: 5 September 2024

References

Ait-Mou, Y., K. Hsu, G.P. Farman, M. Kumar, M.L. Greaser, T.C. Irving, and P.P. de Tombe. 2016. Titin strain contributes to the Frank-Starling law of the heart by structural rearrangements of both thin- and thick-filament proteins. *Proc. Natl. Acad. Sci. USA*. 113:2306–2311. https://doi.org/10.1073/pnas.1516732113

Anderson, R.L., D.V. Trivedi, S.S. Sarkar, M. Henze, W. Ma, H. Gong, C.S. Rogers, J.M. Gorham, F.L. Wong, M.M. Morck, et al. 2018. Deciphering the super relaxed state of human β-cardiac myosin and the mode of action of mavacamten from myosin molecules to muscle fibers. *Proc. Natl. Acad. Sci. USA*. 115:E8143–E8152. https://doi.org/10.1073/pnas.1809540115

Bers, D.M., C.W. Patton, and R. Nuccitelli. 2010. A practical guide to the preparation of Ca(2+) buffers. *Methods Cell Biol.* 99:1–26. https://doi.org/10.1016/B978-0-12-374841-6.00001-3

Brunello, E., and L. Fusi. 2023. Regulating striated muscle contraction: Through thick and thin. *Annu. Rev. Physiol.* 86:255–275. https://doi.org/10.1146/annurev-physiol-042222-02272

Brunello, E., L. Fusi, A. Ghisleni, S.J. Park-Holohan, J.G. Ovejero, T. Narayanan, and M. Irving. 2020. Myosin filament-based regulation of the dynamics of contraction in heart muscle. *Proc. Natl. Acad. Sci. USA*. 117:8177–8186. https://doi.org/10.1073/pnas.1920632117

Caremani, M., E. Brunello, M. Linari, L. Fusi, T.C. Irving, D. Gore, G. Piazzesi, M. Irving, V. Lombardi, and M. Reconditi. 2019a. Low temperature traps myosin motors of mammalian muscle in a refractory state that prevents activation. *J. Gen. Physiol.* 151:1272–1286. https://doi.org/10.1085/jgp.201912424

Caremani, M., F. Pinzauti, J.D. Powers, S. Governali, T. Narayanan, G.J.M. Stienen, M. Reconditi, M. Linari, V. Lombardi, and G. Piazzesi. 2019b. Inotropic interventions do not change the resting state of myosin motors during cardiac diastole. *J. Gen. Physiol.* 151:53–65. https://doi.org/10.1085/jgp.201812196

Caremani, M., L. Fusi, M. Reconditi, G. Piazzesi, T. Narayanan, M. Irving, V. Lombardi, M. Linari, and E. Brunello. 2023. Dependence of myosin filament structure on intracellular calcium concentration in skeletal muscle. *J. Gen. Physiol.* 155:e202313393. https://doi.org/10.1085/jgp.202313393

Coppini, R., C. Ferrantini, A. Mugelli, C. Poggesi, and E. Cerbai. 2018. Altered Ca^{2+} and Na^{+} homeostasis in human hypertrophic cardiomyopathy: Implications for arrhythmogenesis. *Front. Physiol.* 9:1391. https://doi.org/10.3389/fphys.2018.01391

Dong, W., S.S. Rosenfeld, C.K. Wang, A.M. Gordon, and H.C. Cheung. 1996. Kinetic studies of calcium binding to the regulatory site of troponin C from cardiac muscle. *J. Biol. Chem.* 271:688–694. https://doi.org/10.1074/jbc.271.2.688

Dutta, D., V. Nguyen, K.S. Campbell, R. Padrón, and R. Craig. 2023. Cryo-EM structure of the human cardiac myosin filament. *Nature*. 623:853–862. https://doi.org/10.1038/s41586-023-06691-4

Fischetti, R., S. Stepanov, G. Rosenbaum, R. Barrea, E. Black, D. Gore, R. Heurich, E. Kondrashkina, A.J. Kropf, S. Wang, et al. 2004. The BioCAT undulator beamline 18ID: A facility for biological non-crystalline diffraction and X-ray absorption spectroscopy at the Advanced Photon Source. *J. Synchrotron Radiat.* 11:399–405. https://doi.org/10.1107/S0909049504016760

Gillis, T.E., D.A. Martyn, A.J. Rivera, and M. Regnier. 2007. Investigation of thin filament near-neighbour regulatory unit interactions during force development in skinned cardiac and skeletal muscle. *J. Physiol.* 580:561–576. https://doi.org/10.1113/jphysiol.2007.128975

Gong, H.M., W. Ma, M. Regnier, and T.C. Irving. 2022. Thick filament activation is different in fast- and slow-twitch skeletal muscle. *J. Physiol.* 600:5247–5266. https://doi.org/10.1113/JP283574

Gordon, A.M., E. Homsher, and M. Regnier. 2000. Regulation of contraction in striated muscle. *Physiol. Rev.* 80:853–924. https://doi.org/10.1152/physrev.2000.80.2.853

Haselgrove, J.C., and H.E. Huxley. 1973. X-ray evidence for radial cross-bridge movement and for the sliding filament model in actively contracting skeletal muscle. *J. Mol. Biol.* 77:549–568. https://doi.org/10.1016/0022-2836(73)90222-2

Hessel, A.L., W. Ma, N. Mazara, P.E. Rice, D. Nissen, H. Gong, M. Kuehn, T. Irving, and W.A. Linke. 2022. Titin force in muscle cells alters lattice order, thick and thin filament protein formation. *Proc. Natl. Acad. Sci. USA.* 119:e2209441119. https://doi.org/10.1073/pnas.2209441119

Huxley, H.E., and W. Brown. 1967. The low-angle x-ray diagram of vertebrate striated muscle and its behaviour during contraction and rigor. *J. Mol. Biol.* 30:383–434. https://doi.org/10.1016/S0022-2836(67)80046-9

Irving, M. 2017. Regulation of contraction by the thick filaments in skeletal muscle. *Biophys. J.* 113:2579–2594. https://doi.org/10.1016/j.bpj.2017.09.037

Irving, T., Y. Wu, T. Bekyarova, G.P. Farman, N. Fukuda, and H. Granzier. 2011. Thick-filament strain and interfilament spacing in passive muscle: Effect of titin-based passive tension. *Biophys. J.* 100:1499–1508. https://doi.org/10.1016/j.bpj.2011.01.059

Jani, V.P., T. Song, C. Gao, H. Gong, S. Sadayappan, D.A. Kass, T.C. Irving, and W. Ma. 2024. The structural OFF and ON states of myosin can be decoupled from the biochemical super- and disordered-relaxed states. *PNAS Nexus*. 3:pgae039. https://doi.org/10.1093/pnasnexus/pgae039

Jiratrakanvong, J., J. Shao, J. Li, M. Menendez Alvarez, X. Li, P. Das, G. Nikseresht, N. Miskin, R. Huo, J. Nabon, et al. 2024. MuscleX: Data analysis software for fiber diffraction patterns from muscle. *J. Synchrotron Radiat.* 31:1401–1408. https://doi.org/10.1107/S1600577524006167

Köhler, J., Y. Chen, B. Brenner, A.M. Gordon, T. Kraft, D.A. Martyn, M. Regnier, A.J. Rivera, C.K. Wang, and P.B. Chase. 2003. Familial hypertrophic cardiomyopathy mutations in troponin I (K183D, G203S, K206Q) enhance filament sliding. *Physiol. Genomics*. 14:117–128. https://doi.org/10.1152/physiolgenomics.00101.2002

Korte, F.S., E.R. Feest, M.V. Razumova, A.Y. Tu, and M. Regnier. 2012. Enhanced Ca^{2+} binding of cardiac troponin reduces sarcomere length dependence of contractile activation independently of strong crossbridges. *Am. J. Physiol. Heart Circ. Physiol.* 303:H863–H870. https://doi.org/10.1152/ajpheart.00395.2012

Labeit, D., K. Watanabe, C. Witt, H. Fujita, Y. Wu, S. Lahmers, T. Funck, S. Labeit, and H. Granzier. 2003. Calcium-dependent molecular spring elements in the giant protein titin. *Proc. Natl. Acad. Sci. USA.* 100:13716–13721. https://doi.org/10.1073/pnas.2235652100

Linari, M., E. Brunello, M. Reconditi, L. Fusi, M. Caremani, T. Narayanan, G. Piazzesi, V. Lombardi, and M. Irving. 2015. Force generation by skeletal muscle is controlled by mechanosensing in myosin filaments. *Nature*. 528:276–279. https://doi.org/10.1038/nature15727

Little, S.C., B.J. Biesiadecki, A. Kilic, R.S. Higgins, P.M. Janssen, and J.P. Davis. 2012. The rates of Ca^{2+} dissociation and cross-bridge detachment from ventricular myofibrils as reported by a fluorescent cardiac troponin C. *J. Biol. Chem.* 287:27930–27940. https://doi.org/10.1074/jbc.M111.337295

Luo, M., and M.E. Anderson. 2013. Mechanisms of altered Ca^{2+} handling in heart failure. *Circ. Res.* 113:690–708. https://doi.org/10.1161/CIRCRESAHA.113.301651

Ma, W., M. Childers, J. Murray, F. Moussavi-Harami, H. Gong, R. Weiss, V. Daggett, T. Irving, and M. Regnier. 2020. Myosin dynamics during relaxation in mouse soleus muscle and modulation by 2′-deoxy-ATP. *J. Physiol.* 598:5165–5182. https://doi.org/10.1113/JP280402

Ma, W., C.L. Del Rio, L. Qi, M. Prodanovic, S. Mijailovich, C. Zambataro, H. Gong, R. Shimkunas, S. Gollapudi, S. Nag, and T.C. Irving. 2024a. Myosin in autoinhibited off state(s), stabilized by mavacamten, can be recruited in response to inotropic interventions. *Proc. Natl. Acad. Sci. USA.* 121:e2314914121. https://doi.org/10.1073/pnas.2314914121

Ma, W., H. Gong, and T. Irving. 2018a. Myosin head configurations in resting and contracting murine skeletal muscle. *Int. J. Mol. Sci.* 19:2643. https://doi.org/10.3390/ijms19092643

Ma, W., H. Gong, V. Jani, K.H. Lee, M. Landim-Vieira, M. Papadaki, J.R. Pinto, M.I. Aslam, A. Cammarato, and T. Irving. 2022a. Myofibril orientation as a metric for characterizing heart disease. *Biophys. J.* 121:565–574. https://doi.org/10.1016/j.bpj.2022.01.009

Ma, W., H. Gong, B. Kiss, E.J. Lee, H. Granzier, and T. Irving. 2018b. Thick-filament extensibility in intact skeletal muscle. *Biophys. J.* 115:1580–1588. https://doi.org/10.1016/j.bpj.2018.08.038

Ma, W., H. Gong, M. Papadaki, M. Guo, Y. Shao, Q. Qi, R. Liu, J. Zhao, S. Jiang, T. Irving, and J.A. Kirk. 2024b. Evidence for direct regulation of myosin filaments by calcium in intact porcine myocardium. *Biophy J.* 123:316A. https://doi.org/10.1016/j.bpj.2023.11.1946

Ma, W., M. Henze, R.L. Anderson, H. Gong, F.L. Wong, C.L. Del Rio, and T. Irving. 2021. The super-relaxed state and length dependent activation in porcine myocardium. *Circ. Res.* 129:617–630. https://doi.org/10.1161/CIRCRESAHA.120.318647

Ma, W., K.H. Lee, C.E. Delligatti, M.T. Davis, Y. Zheng, H. Gong, J.A. Kirk, R. Craig, and T. Irving. 2023a. The structural and functional integrities of porcine myocardium are mostly preserved by cryopreservation. *J. Gen. Physiol.* 155:e202313345. https://doi.org/10.1085/jgp.202313345

Ma, W., T.S. McMillen, M.C. Childers, H. Gong, M. Regnier, and T. Irving. 2023b. Structural OFF/ON transitions of myosin in relaxed porcine myocardium predict calcium-activated force. *Proc. Natl. Acad. Sci. USA.* 120:e2207615120. https://doi.org/10.1073/pnas.2207615120

Ma, W., S. Nag, H. Gong, L. Qi, and T.C. Irving. 2022b. Cardiac myosin filaments are directly regulated by calcium. *J. Gen. Physiol.* 154:e202213213. https://doi.org/10.1085/jgp.202213213

Matsubara, I. 1980. X-ray diffraction studies of the heart. *Annu. Rev. Biophys. Bioeng.* 9:81–105. https://doi.org/10.1146/annurev.bb.09.060180.000501

Millman, B.M. 1998. The filament lattice of striated muscle. *Physiol. Rev.* 78:359–391. https://doi.org/10.1152/physrev.1998.78.2.359

Nag, S., and D.V. Trivedi. 2021. To lie or not to lie: Super-relaxing with myosins. *Elife*. 10:e63703. https://doi.org/10.7554/eLife.63703

Park-Holohan, S.J., E. Brunello, T. Kampourakis, M. Rees, M. Irving, and L. Fusi. 2021. Stress-dependent activation of myosin in the heart requires thin filament activation and thick filament mechanosensing. *Proc. Natl. Acad. Sci. USA.* 118:e2023706118. https://doi.org/10.1073/pnas.2023706118

Potter, J.D. 1982. Preparation of troponin and its subunits. *Methods Enzymol.* 85 Pt B:241–263. https://doi.org/10.1016/0076-6879(82)85024-6

Reconditi, M. 2006. Recent improvements in small angle X-ray diffraction for the study of muscle physiology. Reports on progress in physics. *Rep. Prog. Phys.* 69:2709–2759. https://doi.org/10.1088/0034-4885/69/10/R01

Reconditi, M., M. Caremani, F. Pinzauti, J.D. Powers, T. Narayanan, G.J. Stienen, M. Linari, V. Lombardi, and G. Piazzesi. 2017. Myosin filament activation in the heart is tuned to the mechanical task. *Proc. Natl. Acad. Sci. USA.* 114:3240–3245. https://doi.org/10.1073/pnas.1619484114

Reconditi, M., L. Fusi, M. Caremani, E. Brunello, M. Linari, G. Piazzesi, V. Lombardi, and M. Irving. 2019. Thick filament length changes in muscle have both elastic and structural components. *Biophys. J.* 116:983–984. https://doi.org/10.1016/j.bpj.2019.02.009

Short, B. 2023. Examining the calcium sensitivity of skeletal muscle thick filaments. *J. Gen. Physiol.* 155:e202313501. https://doi.org/10.1085/jgp.202313501

Spudich, J.A. 2019. Three perspectives on the molecular basis of hypercontractility caused by hypertrophic cardiomyopathy mutations. *Pflugers Arch.* 471:701–717. https://doi.org/10.1007/s00424-019-02259-2

Tobacman, L.S. 1996. Thin filament-mediated regulation of cardiac contraction. *Annu. Rev. Physiol.* 58:447–481. https://doi.org/10.1146/annurev.ph.58.030196.002311

Wang, D., M.E. McCully, Z. Luo, J. McMichael, A.Y. Tu, V. Daggett, and M. Regnier. 2013. Structural and functional consequences of cardiac

troponin C L57Q and I61Q Ca(2+)-desensitizing variants. *Arch. Biochem. Biophys.* 535:68–75. https://doi.org/10.1016/j.abb.2013.02.006

Wang, D., I.M. Robertson, M.X. Li, M.E. McCully, M.L. Crane, Z. Luo, A.Y. Tu, V. Daggett, B.D. Sykes, and M. Regnier. 2012. Structural and functional consequences of the cardiac troponin C L48Q Ca(2+)-sensitizing mutation. *Biochemistry*. 51:4473–4487. https://doi.org/10.1021/bi3003007

Zhao, J., L. Qi, S. Yuan, T.C. Irving, and W. Ma. 2024. Differences in thick filament activation in fast rodent skeletal muscle and slow porcine cardiac muscle. *J. Physiol.* 602:2751–2762. https://doi.org/10.1113/JP286072